Dispersion of particles released at the leading edge of a crop canopy

Ying Pan[a], Marcelo Chamecki[a,*], Scott A. Isard[a], Heidi M. Nepf[b]

[a] *Pennsylvania State University, University Park, PA 16802*
[b] *Massachusetts Institute of Technology, Cambridge, MA 02139*

Abstract

A large-eddy simulation (LES) approach was used to investigate the flow characteristics at a canopy leading edge and their impact on the dispersion of particles released from point sources inside the canopy. Comparison of results from these LES simulations with those for a canopy that is infinite and uniform in both streamwise and spanwise directions reveals important insights about the adjustment lengths for mean flow, turbulent kinetic energy (TKE), and canopy-shear-layer vortices. Two critical locations were identified in the flow adjustment at the leading edge: (1) the location at which canopy-shear-layer vortices begin to develop and (2) the location at which the flow is fully developed. Simulations were conducted for particles released from continuous point sources at four streamwise locations downwind from the leading edge and three heights within the canopy. The four streamwise source locations corresponded to the canopy leading edge, the location at which canopy-shear-layer vortices begin to develop, the transition region, and the fully developed region. The adjustment of flow near the leading edge has a profound impact on the dispersion of particles close to the source, which is where most particle escape from the canopy takes place. Particles released close to the canopy leading edge have much higher maximum escape fractions than particles released in the fully developed region. The adjustment length for particle escape is greater than that for the flow. Away from

*Corresponding author
Email address: chamecki@psu.edu (Marcelo Chamecki)

the source (approximately sixteen canopy heights for the present dense canopy), the geometries of the mean plume become similar for particles released from different regions. Within a few tens of canopy heights from the leading edge, the growth rates of converged mean plume height and depth are lower than those for the case of an infinite canopy.

Keywords: dispersion of particles, canopy edge flow, large-eddy simulation

---

1. Introduction

Many studies of turbulence and dispersion inside and above plant canopies are conducted for canopies that are infinite and uniform in both streamwise and spanwise directions (hereafter referred to as "infinite canopies"). The case of an infinite canopy represents conditions away from canopy edges where flow has adjusted to canopy characteristics (hereafter referred to as "fully developed region", see Fig. 1). When wind blows over vegetated landscapes, the vegetation canopy acts as a displaced wall, inducing rough-wall boundary-layer eddies (*black eddies* in Fig. 1) above the displacement height ($\approx 3/4$ canopy height). Within the canopy, wakes are formed behind individual canopy elements. In addition, surface forces acting on canopy elements produce a net drag force on the air and dissipate the kinetic energy of the air. The presence of a drag force within the canopy and the absence of drag force above the canopy leads to an inflectional mean velocity profile, with the inflection point located near the canopy top. The shape of this canopy-shear-layer profile is similar to that in a free shear layer (mixing layer) formed between two uniform, parallel streams of different velocities (Raupach et al., 1996). The canopy and free shear layers are analogous in the inflectional mean wind profile, consequent flow instabilities, and in the second- and third-order turbulence statistics (Raupach et al., 1996). The non-linear interactions of boundary-layer eddies, canopy-shear-layer vortices (*red eddies* in Fig. 1), and wake eddies lead to an extremely complicated turbulence field within and just above the canopy, a region from the ground to approximately three canopy heights, known as the canopy roughness sublayer

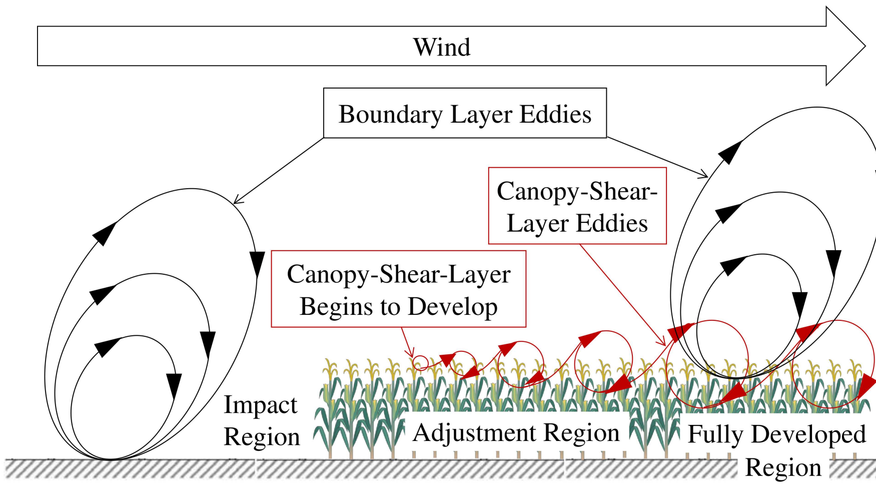

Figure 1: Boundary-layer eddies (*black*) upwind from and above the canopy, and the development of canopy-shear-layer eddies (*red*) beginning a few canopy heights downwind from the leading edge. *Impact, adjustment, and fully developed regions* are labeled.

(Finnigan, 2000; Poggi et al., 2004). The dispersion of scalars and particles within the canopy roughness sublayer usually has a critical contribution from *near-field* dispersion, which is not a Fickian diffusive process and cannot be described by a diffusion equation (Raupach, 1989; Chamecki, 2013). Here *near-field* indicates that the time since particle release is short compared with the Lagrangian time scale (a measure of the coherence or persistence of turbulent motions), and therefore dispersion depends on the velocity histories of the tracer particles (Taylor, 1921; Raupach, 1983). In contrast, dispersion in the *far-field* (for which the time since release is long compared with the Lagrangian time scale) no longer depends on the histories of the tracer particles, and thus becomes a diffusive process that can be described by a diffusion equation (Taylor, 1921; Raupach, 1983).

A recent large-eddy simulation (LES) study successfully reproduced both the turbulence statistics up to the third order and the three-dimensional (3-D) mean particle concentration field during a point-source *Lycopodium* spore release experiment conducted far from the edges of a large maize field (Pan et al., 2014a). However, a description of turbulence and dispersion within and above infinite canopies is insufficient for most environmental applications, because most landscapes are a patchwork of different vegetation types and land uses. In many regions, the fields are small compared to the flow adjustment length at the edge of the canopy, and therefore a large portion of the landscape is occupied by field edge. Understanding the transport processes at the canopy edge is therefore critical for interpreting flux measurements of sensible heat, water vapour, CO_2, and air pollutants (Lee, 2000), as well as estimating the dispersal of biogenic particles such as pollens (Di-Giovanni and Kevan, 1991) and spores (McCartney, 1994). In particular, measurements suggest that pathogenic fungal spores released at the canopy leading edge (transition from flat ground to a single vegetation type) tend to disperse farther than those released in the centre of the field (McCartney, 1994). This finding implies that infection foci at the canopy leading edge are more likely to develop into disease epidemics than those in the fully developed region.

Turbulent flows downwind from canopy leading edges have been studied using field (Irvine et al., 1997; Van Breugel et al., 1999; Nieveen et al., 2001) and wind tunnel (Judd et al., 1996; Morse et al., 2002) measurements, theoretical models (Belcher et al., 2003), and large-eddy simulation (LES) models (Yang et al., 2006b,a; Dupont and Brunet, 2008a,b, 2009). Belcher et al. (2003) suggested that the leading edge flow could be divided into five regions based on the characteristics of mean flow and downward momentum flux: (1) the *impact region* located upwind from the edge, (2) the *adjustment region* within the canopy where the flow is decelerated by canopy drag, (3) the *canopy interior region* where the canopy drag is balanced by downward momentum flux, (4) the *canopy shear layer* at the canopy top where coherent structures develop, and (5) the *roughness-change region* above the canopy where the internal boundary layer (IBL) develops (see Belcher et al., 2003, Fig.3). An important parameter in their model is the canopy-drag length scale, L_c, representing the length scale of which the canopy dissipates the kinetic energy of the flow (Belcher et al., 2003, 2008). LES results of Dupont *et al.* (2009) suggest four stages in the development of coherent structures near the canopy leading edge: (1) *canopy-shear-layer instabilities* develop close to the leading edge due to drag discontinuity at the canopy top, (2) *transverse vortices* form once the canopy-shear-layer instabilities roll over, (3) *two counter-rotating streamwise vortices* appear as secondary instabilities destabilize these rollers, and (4) *complex 3-D coherent structures* develop from the streamwise vortices with spatially constant mean length and separation length scales. The authors used a length scale proportional to the depth of the IBL to characterize the distance occupied by coherent structures in each stage of development. Note that this length scale can also be related to the canopy-drag length scale, because stages develop closer to the leading edge with increasing canopy density (Dupont and Brunet, 2009). One would expect different patterns of particle dispersion for sources located in these regions of distinct flow characteristics.

The objective of this work is to use an LES model to further investigate the flow structure at the canopy leading edge and to explore its impact on the dispersion of particles released from points sources inside the canopy. The LES model is described in Section 2. The adjustment of the flow above and within the canopy is the focus of Section 3, with an emphasis on examining the adjustment lengths for mean flow, turbulent kinetic energy (TKE), and canopy-shear-layer coherent structures. The influence of source location on the dispersion of particles is investigated in Section 4, focusing on the geometry of the mean plume and the escape of particles from the canopy. Effects of mean vertical advection and canopy-shear-layer vortices on the growth of mean plume height and the ground deposition of particles are discussed in Section 5. Conclusions are presented in Section 6.

2. Numerical model

The LES model employed in this work was described in detail in Pan et al. (2014a,b). The model solved the 3-D conservation equations of fluid momentum and particle concentration, implying that a continuous concentration field was advected by a continuous velocity field. Coriolis force and buoyancy effects were not considered. The most important effect of the canopy on the airflow was to exert a drag force that dissipates the kinetic energy of the air. A distributed drag force ($\boldsymbol{f}_D$) was used to represent the surface forces exerted by canopy elements within the grid volume and was parameterized following the standard practice in LES studies,

$$\boldsymbol{f}_D = -C_D\,(a\mathbf{P}) \cdot (|\tilde{\boldsymbol{u}}|\tilde{\boldsymbol{u}})\,. \tag{1}$$

Here $\tilde{\boldsymbol{u}}$ is the filtered velocity, $a\boldsymbol{P}$ is the two-sided leaf area density (a; Fig. 2) split into streamwise (x), spanwise (y), and vertical (z) directions using a diagonal second-order projection tensor ($\mathbf{P}$). The value of $\mathbf{P} = P_x \boldsymbol{e}_x \boldsymbol{e}_x + P_y \boldsymbol{e}_y \boldsymbol{e}_y + P_z \boldsymbol{e}_z \boldsymbol{e}_z$ ($P_x = P_y = 0.28$, $P_z = 0.44$) was provided by Pan et al. (2014a) using measurements of maize canopies (Wilson et al., 1982; Bouvet et al., 2007). The model of drag coefficient, $C_D = \min\left((|\tilde{\boldsymbol{u}}|/A)^B, C_{D,\max}\right)$ ($A = 0.22$ m s^{-1}, $B = -2/3$, and $C_{D,\max} = 0.8$), was proposed by Pan et al. (2014b) to represent simple bending of leaves and stems of maize plants. For low velocity, bending is negligible, and the drag coefficient remains approximately constant ($C_D = C_{D,\max}$). For high velocity, bending is strong, and the drag coefficient follows a power-law decay with increasing velocity ($C_D = (|\tilde{\boldsymbol{u}}|/A)^B$). Dimensional analysis has suggested that $B = -2/3$ for strong one-dimensional (1-D) bending (Alben et al., 2002; de Langre et al., 2012). Values of A and $C_{d,\max}$ were fitted using mean velocity and mean momentum flux profiles (Gleicher et al., 2014).

The 3-D momentum equations were solved using a fully dealiased, pseudo-spectral approach in the horizontal directions and a second-order, centered, finite-difference scheme in the vertical direction. The equations were closed using the Lagrangian scale-dependent dynamics Smagorinsky subgrid-scale (SGS) model (Bou-Zeid et al., 2005). The conservation of particle concentration was discretized using a finite-volume scheme with a third-order bounded scheme for the advection term (Chamecki et al., 2008). Following Chamecki et al. (2009), the advective velocity for the particle concentration field was approximated as

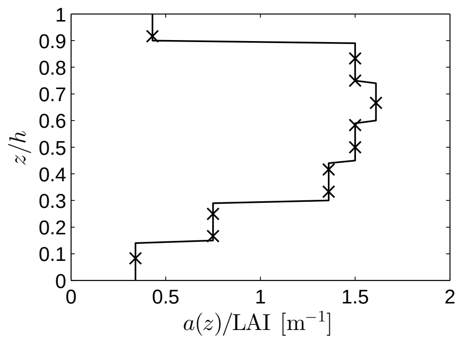

Figure 2: Two-sided leaf area density, $a(z)$, normalized by one-sided leaf area index (LAI) for heights (z) normalized by canopy height (h), measured by Wilson et al. (1982) for a cornfield (*solid line*). Here LAI = 3.3 was measured by Gleicher et al. (2014) for the maize field of interest. *Crosses* indicate the values of $a(z)$ on the LES grid for horizontal velocity components.

the superposition of the instantaneous fluid velocity and a constant particle settling velocity ($w_s = 0.0194$ m s^{-1} for Lycopodium spores (Ferrandino and Aylor, 1984)). The effect of particle inertia was neglected because only particles with small Stokes numbers were employed in the simulations (Pan et al., 2013). The SGS particle flux was modeled using an eddy-diffusivity approach and a constant SGS Schmidt number ($Sc_{\mathrm{SGS}} = 0.4$) (Chamecki et al., 2009). The rate of particle deposition on the ground was parameterized using a wall model with specified zero concentration at the ground roughness height. The rate of particle deposition on canopy elements was estimated using a modified version of the model described by Aylor and Flesch (2001), accounting for gravitational settling, impaction, re-entrainment and rebound of particles (see Pan et al., 2014a, Appendix A).

A total of 12 LES runs were performed to study turbulence and particle dispersion downwind from a canopy leading edge. As shown in Fig. 3, the simulation domain is a box with $L_x \times L_y \times L_z = 44.3h \times 20h \times 10h$ discretized using $186 \times 84 \times 120$ grid points respectively, where $h = 2.1$ m is the maize canopy height. The modeled canopy occupied $24h$ of the streamwise domain ($0 \leq x/h \leq 24$, corresponding to grid points 34–135), the entire spanwise domain (L_y), and the first 12 vertical layers. The flow field was driven by an imposed mean pressure gradient, and a no-stress boundary condition was imposed at the top of the domain. Note that the no-stress boundary condition at $z/h = 10$ (the top of the domain) is unrealistic. Nevertheless, turbulence statistics within the canopy layer and the IBL are not significantly affected by this feature because, in the canopy and roughness sublayer, turbulence attributes are mostly determined by the interaction with the plant canopy (Bailey and Stoll, 2013; Pan et al., 2014a). A wall model was used to parameterize the bottom boundary condition at the ground beneath the plants (with roughness length $z_0 = 0.01$ m). In order to avoid effects of canopy wake on the inflow, an inflow boundary condition at the beginning of the domain was provided by a precursor simulation with the same configuration but without plants. The inflow was imposed at $8h$ upwind from the canopy leading edge. This distance is larger than the length scale of the impact region proposed by Belcher et al. (2003) and Rominger and Nepf (2011), and therefore the inflow condition is unlikely to be affected by the plant canopy downwind. The last $4h$ of the domain (grid points 169–186, beginning $8.3h$ downwind from the canopy trailing edge) was used as a fringe region (Chester et al., 2007) to force the velocity field back to the inflow boundary condition. This allowed simulation of non-periodic flow in the streamwise direction using pseudospectral numerics. The spin-up of the flow field consisted of a first stage lasting 32 minutes that allowed the velocity field to develop fully in the absence of the canopy and a second 40-minute long stage that enabled the mean flow and turbulence to adjust to the presence of the canopy and reach a statistically steady state. The 12 runs, each lasting for 1.2 hours, used the same spin-up and inflow boundary condition. Particles were continuously released from point sources at streamwise locations $x_{\mathrm{src}}/h = 0$, 1.9, 9, and 13.6, and vertical locations at $z_{\mathrm{src}}/h = 1$, 2/3, and 1/3 for each x_{src} (subcript "src" represents "source"). A snapshot of the concentration field for particles released at ($x_{\mathrm{src}}/h = 2$, $z_{\mathrm{src}}/h = 1$) is shown in Fig. 3. Analysis of the flow and concentration fields only considered the last hour of each LES case study, which approximates statistically steady-state conditions.

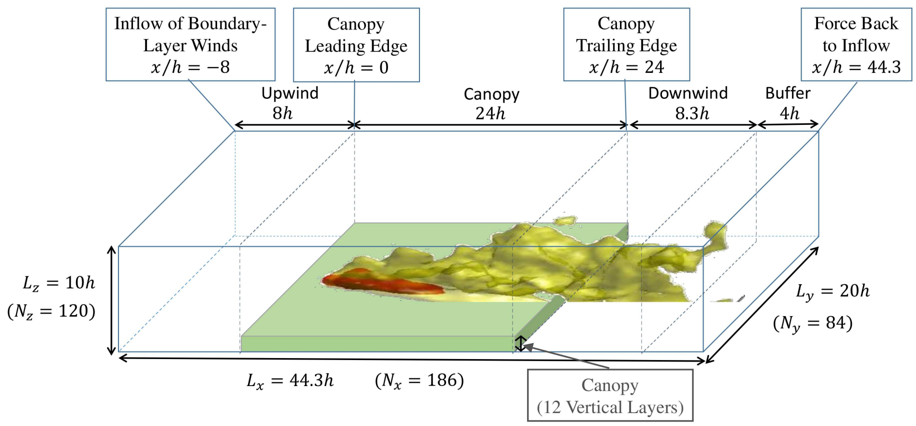

Figure 3: The components of LES domain configuration. The iso-surfaces demonstrate a snapshot of concentration field for particles released at ($x_{\rm src}/h = 2$, $z_{\rm src}/h = 1$). The red and yellow iso-surfaces represent $C/Q = 0.1$ and 0.01 s m^{-3}, respectively. Here C is the particle concentration, and Q is the strength of the continuous point source.

The flow field and particle dispersion were analyzed for the streamwise domain $-4 < x/h < 20$, which extends from the *impact region* to the *fully developed region*. This region of interest is not affected by the canopy trailing edge at $x/h = 24$. The vertical domain of interest is $0 < z/h < 4$, which includes the canopy layer and the IBL. Simulation results were analyzed together with those for an infinite canopy reported by Pan et al. (2014a) to show the effects of the canopy leading edge on turbulence and particle dispersion. The friction velocity within the fully developed region, $u_\star = 0.51$ m s^{-1} (from Pan et al., 2014a) was used as the normalization velocity scale for analysis of results.

3. Flow field downwind from the canopy leading edge

A roughness transition occurs at the canopy leading edge, inducing the development of an internal boundary layer (IBL) above the canopy. Within the IBL, the flow is mainly controlled by the underlying canopy. Well above the canopy ($z/h \gg 1$), the flow is horizontally homogeneous and maintains equilibrium with the upwind surface. This situation, in combination with the low velocities inside the canopy, leads to a larger vertical gradient of mean streamwise velocity ($\partial\overline{u}/\partial z$) above the canopy than occurs above the upwind surface. Thus, the IBL can be identified as the region $(\partial\overline{u}/\partial z)-(\partial\overline{u}/\partial z)_{\text{inflow}} > 0$. Note that in the present configuration, this region defining the IBL is practically indistinguishable from the region $(\partial\overline{u}/\partial z) - (\partial\overline{u}/\partial z)_{\infty} > 0$ (shown in Fig. 4*a*). The *subscript* "∞" indicates results for LES runs using an infinite canopy from Pan et al. (2014a). For the horizontal domain of interest ($x/h \leq 20$), the region of flow strongly modified by the presence of the canopy (including the canopy layer and the IBL) is confined within the region $0 < z/h < 4$. The growth of the IBL is consistent with that reported by Dupont and Brunet (2009), with IBL depth becoming similar to the canopy height at $x/h = 6$ and reaching twice the canopy height by $x/h = 20$, beyond which it continues to grow.

At the canopy leading edge, the mean streamwise velocity ($\overline{u}$; Fig. 4*b*) decelerates as a consequence of canopy drag, transitioning from a boundary-layer-type mean wind profile to a canopy-shear-layer-type, inflected mean wind profile in the fully developed region. The only exception is the region of $\partial\overline{u}/\partial x > 0$ observed close to the canopy leading edge in the lower half of the canopy ($-0.2 < x/h < 1.2$, $z/h < 1/2$; Fig. 4*c*). This is caused by the relatively low leaf area density near the ground that channels part of the flow deflected from the high leaf area density in the upper canopy. The mean flow within the canopy is considered fully adjusted to the canopy drag when the streamwise gradient of $\overline{u}$ becomes negligible ($|\partial\overline{u}/\partial x|/(u_\star/h) < 0.1$; *white region* in Fig. 4*c*). Here the adjustment length for $\overline{u}$ is observed to be $x/h \approx 16$.

Vertical transport of particles is impacted by mean and fluctuating components of vertical velocity. From continuity, the mean vertical velocity depends on the streamwise gradient of mean streamwise velocity,

$$\overline{w}(z) = -\int_0^z (\partial\overline{u}/\partial x)\, dz. \tag{2}$$

The deceleration of $\overline{u}$ leads to significant positive mean vertical velocity ($\overline{w}/u_\star > 0.1$) within and above the canopy for $x/h < 13$ (Fig. 5*a*). Negative mean vertical velocity is observed close to the canopy leading edge in the lower half

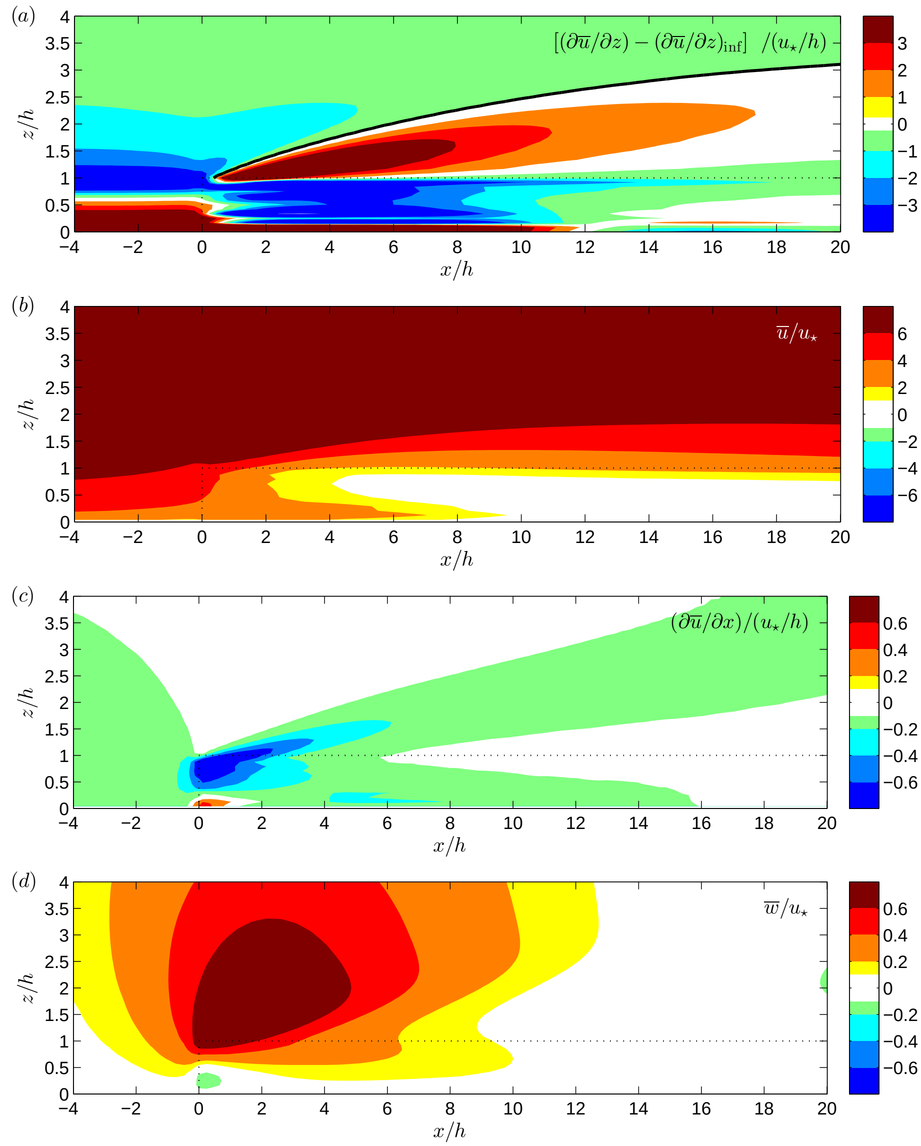

Figure 4: Iso-contours of normalized vertical velocity gradient of mean streamwise velocity with respect to the case of an infinite canopy ($[(\partial\overline{u}/\partial z)-(\partial\overline{u}/\partial z)_\infty]/(u_\star/h)$; a), normalized mean streamwise velocity ($\overline{u}/u_\star$; b), normalized streamwise gradient of mean streamwise velocity ($(\partial\overline{u}/\partial x)/(u_\star/h)$; c), and normalized mean vertical velocity ($\overline{w}/u_\star$; d) plotted in x/h (downwind) and z/h (vertical) space. Canopy edge ($x/h=0$, $z/h<1$) and top ($x/h>0$, $z/h=1$) are indicated using *dotted lines*. White regions in each panel indicate $|[(\partial\overline{u}/\partial z)-(\partial\overline{u}/\partial z)_\infty]/(u_\star/h)|<0.25$ (a), $|\overline{u}|/u_\star<1$ (b), $|\partial\overline{u}/\partial x|/(u_\star/h)<0.1$ (c), and $|\overline{w}|/u_\star<0.1$ (d), respectively. The development of IBL is identified as the region $\partial\overline{u}/\partial z-(\partial\overline{u}/\partial z)_\infty>0$ above the canopy ($z/h>1$), with the IBL height represented by the *solid black line* in (a). The *subscript* "∞" indicates results for LES runs using an infinite canopy reported by Pan et al. (2014a).

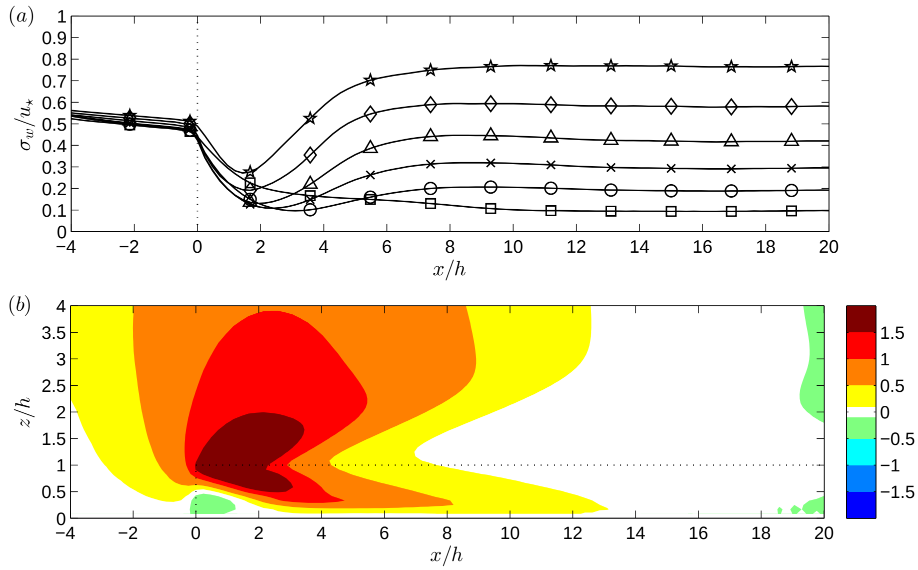

Figure 5: (a) Normalized standard deviation of vertical velocity $(\sigma_w/u_\star)$ within the canopy against normalized downwind distance from the leading edge (x/h) at different heights represented by *lines with different symbols*: $z/h = 1$ (*pentagrams*), 5/6 (*diamonds*), 2/3 (*triangles*), 1/2 (*crosses*), 1/3 (*circles*), and 1/6 (*squares*). (b) The ratio between mean and standard deviation of vertical velocity $(\overline{w}/\sigma_w)$ plotted in x/h (downwind) and z/h (vertical) space. White region in (b) indicates $|\overline{w}|/\sigma_w < 0.1$.

of the canopy $(-0.2 < x/h < 1.2,\ z/h < 1/2)$ associated with the streamwise acceleration of streamwise velocity.

The intensity of turbulent fluctuation of vertical velocity is measured by its standard deviation, σ_w. Fig. 5(a) shows that σ_w within the canopy becomes nearly independent of downwind distance from the leading edge at $x/h \approx 10$. Inspection of Fig. 5(b) suggests that the mean vertical velocity at a downwind distance of $x/h \approx 13$ becomes negligible with respect to the intensity of its turbulent fluctuation $(|\overline{w}|/\sigma_w < 0.1)$.

The increasing value of σ_w with downwind distance near the leading edge (at $2 < x/h < 10$ in Fig. 5b) reveals the increase of the strength of the canopy-shear-layer vortices. The size of canopy-shear-layer vortices also increases with downwind distance from the leading edge, characterized by the shear length scale,

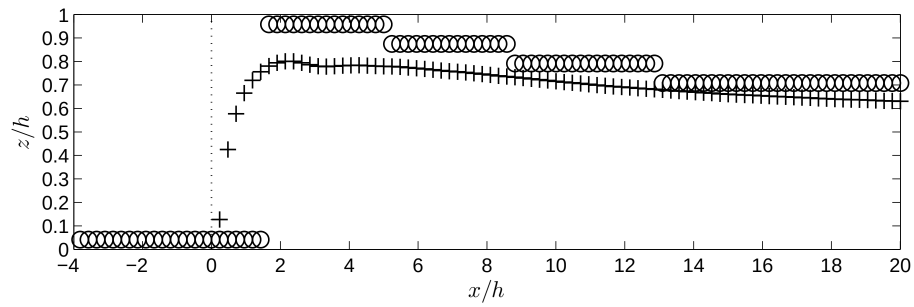

Figure 6: The penetration depth of shear ($1 - L_s/h$; *plus signs*) and the peak location of the skewness of streamwise velocity ($z(Sk_{u,\max})$; *circles*) against downwind distance from the leading edge (x/h). Here $L_s = \overline{u}_h/(\partial\overline{u}/\partial z)_h$ is the shear length scale, and *subscript* "h" indicates values at the canopy top.

$L_s = \overline{u}_h/(\partial\overline{u}/\partial z)_h$ (Raupach et al., 1996). Investigating mean wind profiles at each streamwise grid (not shown) suggests that the inflectional mean wind profile first appears at $x/h \approx 2$, where the value of L_s reaches a minimum (*plus signs* in Fig. 6). The canopy-shear-layer vortices only develop beyond this point (Dupont and Brunet, 2009), and the growth of these vortices with downwind distance is revealed by the increase of L_s. Pan et al. (2014b) proposed an alternative measure of the size of canopy-shear-layer vortices: the vertical position of the peak in the vertical profile of streamwise velocity skewness ($z(Sk_{u,\max})$; *circles* in Fig. 6). When boundary layer winds approach the canopy leading edge, an abrupt jump of $z(Sk_{u,\max})$ from the ground to the canopy top is observed at $x/h \approx 2$. This is consistent with the downwind distance required for the formation of canopy-shear-layer vortices suggested by the minimum of L_s. At $x/h > 2$, $z(Sk_{u,\max})$ decreases with x/h until reaching the value reported for the case of an infinite canopy (Pan et al., 2014b) at $x/h = 13.3$, and thereafter remains constant. This trend in $z(Sk_{u,\max})$ suggests that canopy-shear-layer vortices grow and increase their penetration before reaching a fully developed state at $x/h = 13.3$. Note that the downward steps in the *circles* (Fig. 6) are due to a vertical grid size of $h/12$.

To review, the adjustment length scale within the canopy exhibits some variation among the different flow statistics (e.g., $x/h \approx 16$ for $\overline{u}$ from Fig. 4(b), $x/h \approx 10$ for σ_w from Fig. 5(a), $x/h \approx 13$ for $\overline{w}/\sigma_w$ from Fig. 5(b), and $x/h \approx 13.3$ for $z(Sk_{u,\max})$ from Fig. 6). The adjustment lengths suggested by $\overline{u}$, σ_w and $\overline{w}/sigma_w$ depend on the choice of cut-off values (e.g., the cut-off for $\overline{w}/\sigma_w$ is 0.1). Compared with these metrics, the metric of $z(Sk_{u,\max})$ is more robust because it does not depend on a selected cut-off. Thus we choose the adjustment length scale for $z(Sk_{u,\max})$ as a representative value for all the processes, with an uncertainty range of ± 3 canopy heights suggested by other metrics. Vertical profiles of mean streamwise velocity, mean vertical momentum flux, as well as standard deviation and skewness of velocity components within the region $13.3 < x/h < 20$ (not shown) agree well with those obtained for the case of an infinite canopy (Pan et al., 2014a,b).

So far, the results of flow adjustment have suggested two critical locations downwind from the canopy leading edge: (1) $x/h = 2 \pm 0.2$, where canopy-shear-layer vortices begin to develop, and (2) $x/h \pm 13.3 \pm 3$, where the flow is fully developed. For the purpose of extending to other types of canopies, the canopy-drag length scale, L_c, is a more appropriate scale than the canopy height. Specifically, it is the integrated canopy drag, and not just the canopy height, that controls the adjustment in flow momentum. The canopy-drag length scale is defined as $L_c = h/(\overline{C}_D P_x \int_0^h a(z)dz)$. Here $\overline{C}_D = 0.25$ is the depth-averaged canopy drag coefficient in the fully developed region, $P_x = 0.28$ is the ratio between frontal and total leaf area densities, and $\int_0^h a(z)dz = 7.7$ is the depth-integrated two-sided leaf area index. These values yield $L_c = 1.9h$ for the present canopy. Consequently the two critical downwind locations correspond to $x/L_c = 1 \pm 0.1$ and $x/L_c = 7 \pm 1.5$. The downwind distance $x/L_c = 7 \pm 1.5$ is in reasonable agreement with the theoretical estimate of adjustment length proposed by Chen et al. (2013), $x/L_c = \beta(1 + 2\alpha h/L_c) = 5.3 \pm 1.1$, where $\beta = 1.5 \pm 0.2$ and $\alpha = 2.3 \pm 0.2$.

In order to facilitate the description of particle dispersion in the next section, we divide the canopy in our study into six regions of different flow characteristics. As shown in Fig. 7, these regions are defined by the boundaries $x/L_c = 1$,

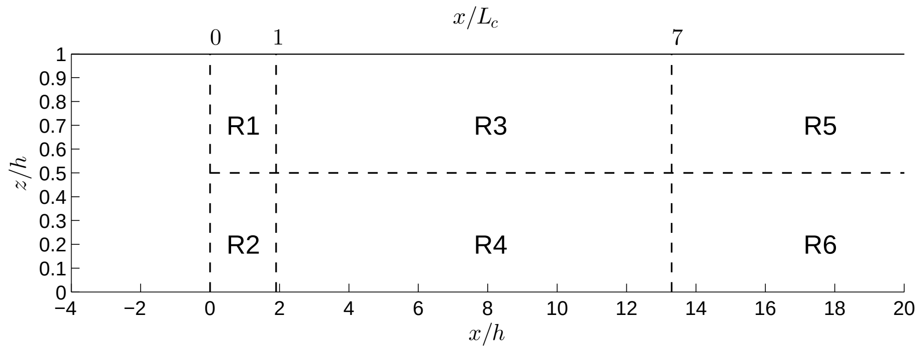

Figure 7: The field downwind from a canopy leading edge is divided into six regions of different flow characteristics. Note that the streamwise extent of the region is defined using x/L_c, which may correspond to different values of x/h for other canopies. Here x is the downwind distance from the canopy leading edge, z is the height above the ground, h is the canopy height, and L_c is the canopy-drag length scale (Belcher et al., 2003).

$x/L_c = 7$ and $z/h = 1/2$. Before the development of canopy-shear-layer vortices, strong positive mean vertical velocity characterizes the upper canopy region (R1), in contrast to the weak (negative and positive) mean vertical velocity observed in the lower canopy region (R2). In the fully developed region, the vertical transport of particles is dominated by canopy-shear-layer vortices, but by different types of events in the upper (R5) and lower (R6) canopies (see detailed discussion in Section 5). Note that the separation of upper and lower canopy regions at $z/h = 1/2$ was determined qualitatively. In reality, it should depend on the vertical distribution of leaf area density.

4. Effects of canopy leading edge on dispersion of particles

In order to investigate the effects of the canopy leading edge on dispersion of particles, simulations were conducted for continuous point-source release at four streamwise locations ($x_{\mathrm{src}}/h = 0$, 1.9, 9, and 13.6) and three heights ($z_{\mathrm{src}}/h = 1$, 2/3, and 1/3). The four streamwise locations correspond to the canopy leading edge ($x/h = 0$; beginning of R1 and R2), the location where canopy-shear-layer vortices begin to develop ($x/L_c = 1$; end of R1 and R2), the transition region ($1 < x/L_c < 7$; R3 and R4), and the fully developed region ($x/L_c > 7$; R5 and R6). The focus of this work is on the vertical dispersion of particles released inside the canopy near the leading edge. The vertical and horizontal distribution of the cross-wind integrated mean concentration field ($\chi(x,z) = \int_y \overline{C} dy$) is analyzed in Section 4.1. Escape fraction and particle deposition are studied in Section 4.2.

4.1. The growth of the mean plume

Fig. 8 depicts the spatial distribution of the cross-wind integrated mean concentration field ($\chi(x,z) = \int_y \overline{C} dy$) scaled by the strength of the continuous point source (Q) for particles released at $z_{\mathrm{src}}/h = 2/3$ and $1/3$. Note that the unit of χ/Q is s m^{-2}. We use the behaviour of the iso-contour $\chi/Q = 0.1$ s m^{-2} to discuss qualitative aspects of the plume. The downwind distance $(x - x_{\mathrm{src}})$, to which the iso-contour of $\chi/Q = 0.1$ s m^{-2} stretches provides a measure of particle dispersal distance. These iso-contours entend farther from the source for particles released close to the leading edge (Fig. 8*a*–*d*) than those for particles released far from the leading edge (Fig. 8*e*–*h*). This trend is in agreement with the observation that particles released at the canopy leading edge tend to disperse farther downwind than those released in the centre of the field (McCartney, 1994). Similarly, the growth of the particle plume can be inferred from the stretch of the iso-contour $\chi/Q = 0.1$ s m^{-2} in the vertical direction. For particles released in R1 (Fig. 8*a*, *c*), the iso-contours are arched, demonstrating the effect of strong positive mean vertical velocity in this region. Similar arched iso-contours are also observed for particles released at $z_{\mathrm{src}}/h = 1$ (not shown).

Quantitatively the growth of the plume can be characterized by the mean height (*dots* in Fig. 8),

$$\overline{z}(x) = \frac{\int_{z=0}^{z\to\infty} z\chi(x,z)dz}{\int_{z=0}^{z\to\infty} \chi(x,z)dz}, \tag{3}$$

and the standard deviation of vertical mass distribution, which is a measure of

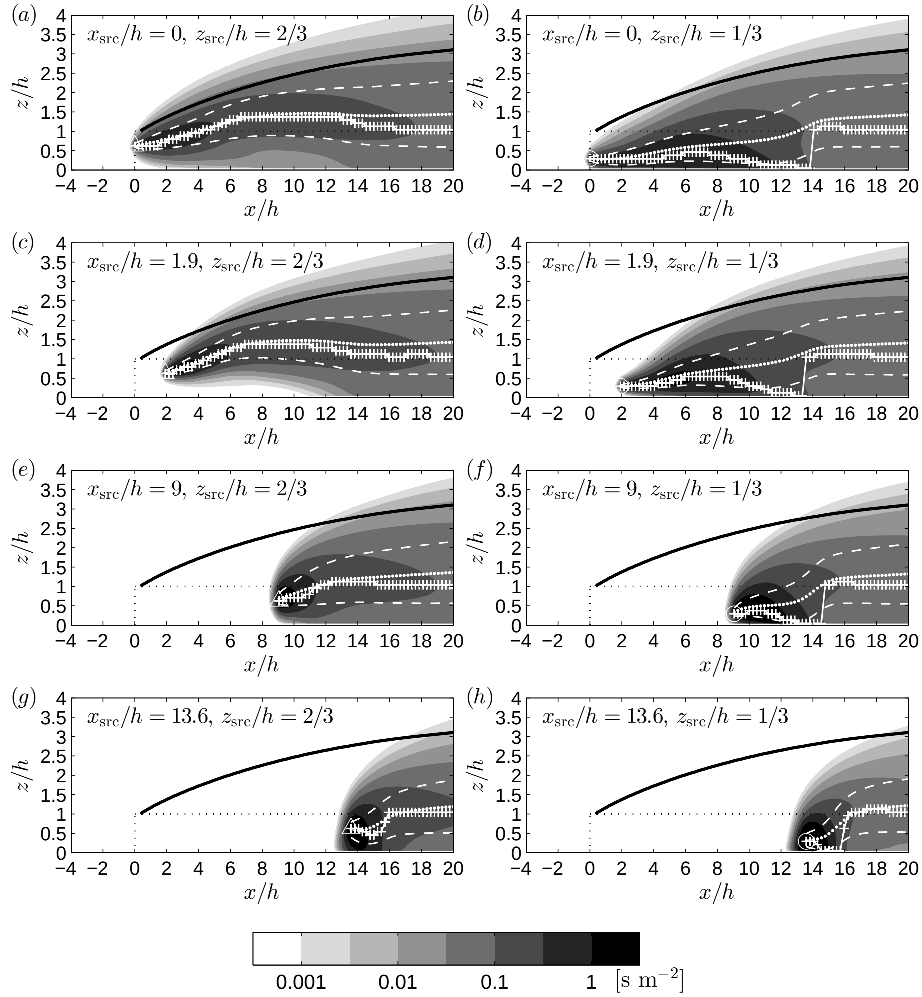

Figure 8: Iso-contours of mean concentration integrated in the crosswind direction (χ) normalized by the strength of the continuous point source (Q) plotted in x/h (downwind) and z/h (vertical) space for particles released at four streamwise locations ($x_{\mathrm{src}}/h = 0$ (a, b), 1.9 (c, d), 9 (e, f), and 13.6 (g, h)) and two heights ($z_{\mathrm{src}}/h = 2/3$ (a, c, e, f) and 1/3 (b, d, f, h)). *Triangles and circles* indicate point sources located at $z_{\mathrm{src}}/h = 2/3$ and 1/3, respectively. *Black solid lines* indicate the IBL height determined as $\partial\overline{u}/\partial z = (\partial\overline{u}/\partial z)_\infty$ (see Fig. 4a), where *subscript* "∞" indicates LES results using an infinite canopy reported by Pan et al. (2014a). *White dots, dash lines, and plus signs* indicate results for $\overline{z}/h$, $(\overline{z} \pm \sigma_z)/h$, and the location of maximum $\chi(x, z)$ at a given x ($z_{\max}$), respectively.

mean plume depth,

$$\sigma_z(x) = \left(\frac{\int_{z=0}^{z\to\infty} (z-\overline{z})^2 \chi(x,z) dz}{\int_{z=0}^{z\to\infty} \chi(x,z) dz} \right)^{1/2} = (\overline{z^2} - \overline{z}^2)^{1/2}. \tag{4}$$

By definition 68% of the particles are confined to the region $\overline{z} \pm \sigma_z$ (between the two *dash lines* in Fig. 8). The location of the maximum cross-wind integrated mean concentration ($z_{\max}$) coincides with the centroid of the plume ($\overline{z}$) within a limited downwind distance from the source, and then deviates from $\overline{z}$ as the plume becomes increasingly skewed (compare *plus signs* ($z_{\max}$) and *dots* ($\overline{z}$) in Fig. 8). For release in the lower canopy ($z_{\text{src}}/h = 1/3$), an abrupt jump of $z_{\max}$ from the ground to the canopy top occurs downwind from the source. The downwind distance ($x - x_{\text{src}}$) at which the jump occurs decreases as the source is moved downwind from the leading edge.

Fig. 9 shows mean plume height ($\overline{z}$) and depth (σ_z) against downwind distance from the source ($x - x_{\text{src}}$). The mean plume depth (σ_z; Fig. 9*b*) is affected by the intensity of vertical turbulent transport (characterized by σ_w). As shown in Fig. 5*a*, σ_w increases with downwind distance from the leading edge and approaches a constant value at $x/h \approx 10$. Therefore particles released away from the leading edge (*cyan and blue lines*) produce plumes with larger σ_z than those released close to the edge ($x_{\text{src}}/h < 2$; *red and green lines*). Both $\overline{z}$ and σ_z become independent of the release height (z_{src}) at some distance downwind from the source, and this downwind distance is comparable to that observed for the abrupt jump of $z_{\max}$ for the release in the lower canopy ($z_{\text{src}}/h = 1/3$). Both $\overline{z}$ and σ_z tend to become independent of the streamwise release location at $(x - x_{\text{src}})/h \approx 16$, suggesting that the particle plume away from the source is independent of source location. The converged $\overline{z}$ and σ_z values grow as power-law functions of downwind distance from the source ($x - x_{\text{src}}$) with an exponent of approximately 0.2. This exponent value of this exponent is significantly smaller than the power-law exponent 0.5 reported for the case of an infinite canopy (Pan et al., 2014a, see *black lines* in Fig. 9), because the growth of the plume is limited by the development of IBL at the canopy leading edge (shown by *black*

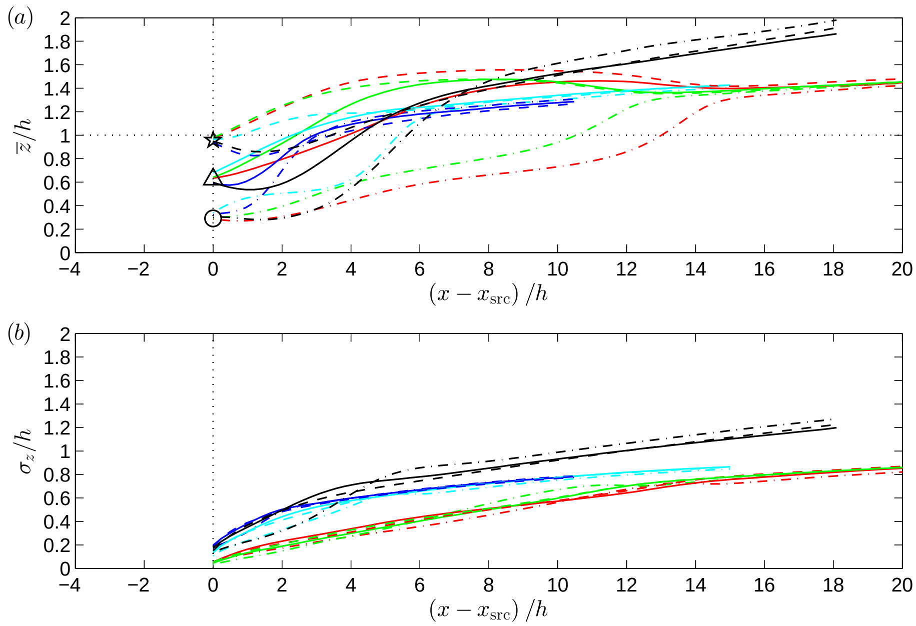

Figure 9: The mean height ($\overline{z}/h$; a) and depth (σ_z/h; b) of the plume against downwind distance from the source ($(x - x_{\rm src})/h$) for particles released at $z_{\rm src}/h = 1$ (*dash lines*), 2/3 (*solid lines*), and 1/3 (*dash-dot lines*). *Red, green, cyan, blue, and black lines* indicate particles released from $x_{\rm src}/h = 0$, 1.9 9, 13.6, and ∞ (the case of an infinite canopy from Pan et al. (2014a)), respectively. *Pentagram, triangle, and circle* indicate point sources located at $z_{\rm src}/h = 1$, 2/3, and 1/3, respectively.

solid lines in Fig. 8). As shown by the mean concentration fields, the majority of particles ($\chi/Q > 0.01$ s m^{-2}) are located below the IBL height. The analytical model presented by Pan et al. (2014a) suggests that the growth rates of $\overline{z}$ and σ_z decrease with increasing mean shear ($\partial\overline{u}/\partial z$). Thus, plume growth at the canopy leading edge is reduced by the enhanced mean shear within the IBL compared with that above an infinite canopy ($(\partial\overline{u}/\partial z) - (\partial\overline{u}/\partial z)_\infty > 0$; Fig. 4$a$). This effect remains significant for particles released at $x_{\rm src}/L_c = 7$ (the farthest release considered in this work).

4.2. Escape fraction and deposition

Fig. 10 shows the fraction of particles that escaped the canopy (EF) and that are removed by deposition on canopy elements (F_{S_p}) and the ground (F_{Φ_G}). These fractions are defined as (Pan et al., 2014a),

$$\mathrm{EF} = \frac{1}{Q}\int_x \int_{z=h}^{z\to\infty} \int_y \overline{uC} dydzdx, \tag{5}$$

$$F_{S_p} = \frac{1}{Q}\int_x \int_{z=0}^{z=h} \int_y \overline{S}_p dydzdx, \tag{6}$$

$$F_{\Phi_G} = \frac{1}{Q}\int_x \int_y \Phi_G dydx. \tag{7}$$

Here $\overline{uC}$ is the mean concentration flux in the streamwise direction, $\overline{S}_p$ is the mean rate of deposition on canopy elements, Φ_G is the mean rate of deposition on the ground, $\int_x$ indicates integration from $x \to -\infty$ to some arbitrary x, and $\int_y$ indicates integration from $y \to -\infty$ to $y \to \infty$. Fig. 10a shows that most escape occurs within a few canopy heights downwind from the source (within $(x - x_{\mathrm{src}})/h \leq 5$ for the release in the upper canopy ($z_{\mathrm{src}}/h \geq 2/3$; *dash and solid lines*) and within $(x - x_{\mathrm{src}})/h \leq 10$ for the release in the lower canopy ($z_{\mathrm{src}}/h = 1/3$; *dash-dot lines*)). Away from the source ($(x - x_{\mathrm{src}})/h > 10$), most airborne particles are located above the canopy (not shown). Particles being transported within the canopy are quickly depleted by deposition on canopy elements and on the ground, and thus do not contribute to transport beyond a few tens of canopy heights. Studies of long distance transport need an effective source strength that accounts only for particles that have escaped the canopy, i.e., $Q \cdot \mathrm{EF}$. For all cases, the escape fraction peaked before the end of the domain of interest ($x/h = 20$), and the maximum escape fraction ($\mathrm{EF}_{\mathrm{max}}$) is approximately the same as the escape fraction at the end of the domain of interest (Fig. 10a). This behaviour is consistent with the finding from Pan et al. (2014a) that for particles with negligible settling velocity ($w_s/u_\star \approx 0.04 \ll 1$), only a small fraction of particles that have escaped the canopy return to the canopy within a downwind distance of about ten canopy heights from the source.

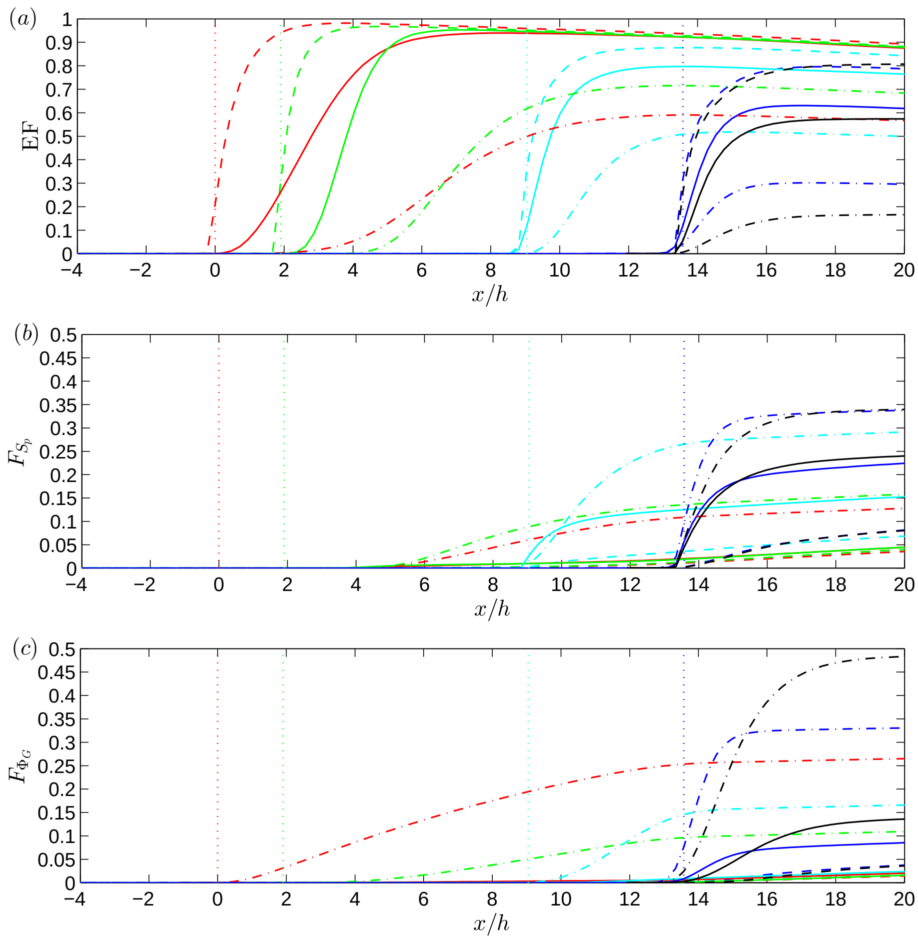

Figure 10: The fractions of particles having escaped the canopy (EF; *a*) and removed by deposition on canopy elements (F_{S_p}; *b*) and the ground (F_{Φ_G}; *c*) against downwind distance from the canopy edge (x/h) for particles released from $x_{\rm src}/h = 0$, 1.9, 9 and 13.6 marked using *vertical dot lines*. *Lines of different styles and colors* are defined in Fig. 9.

Inspection of Fig. 10b reveals that deposition on canopy elements does not occur close to the leading edge ($F_{S_p} \approx 0$ at $x/h < 4$). This feature is caused by the parameterization used in the canopy deposition model, which assumes that rebound and re-entrainment occur when the speed of a particle exceeds a critical value ($V_{\mathrm{crit}} = 0.45$ m s^{-1}, (Aylor and Flesch, 2001)). At $x/h < 4$, particles are transported at sufficiently high speeds by (greater than V_{crit}) within the canopy that they are unlikely to deposit on canopy elements. Because the critical velocity (V_{crit}) is an empirical constant in the current model, changes in wind conditions ($u_\star$) will vary the patterns of particle deposition on canopy elements.

Because the flow at $x/L_c > 7$ is fully adjusted to the crop canopy, the rates of deposition on canopy elements for particles released in R5 and R6 are approximately the same as those for particles released in infinite canopy case (*blue lines* compared with *black lines* in Fig. 10)b). However, only particles released at the top of R5 yield approximately the same escape and ground deposition fractions as those released in the case of an infinite canopy (*blue and black dash lines* in Fig. 10a, c). For release in the fully developed region, as the source height decreases, the escape fraction increases and the ground deposition decreases, relative to the infinite canopy case (*blue and black solid and dash-dot lines* in Fig. 10c, a). In particular, particles released at $z_{\mathrm{src}}/h = 1/3$ yield a value for $\mathrm{EF}_{\max}$ about twice that for particles released in an infinite canopy (0.3 compared with 0.17; *blue and black dash-dot lines* in Fig. 10a). The increase of the adjustment length for particle escape with decreasing release height is consistent with the trend that the adjustment length for mean wind ($\overline{u}$ and $\overline{w}/\sigma_w$) increases with decreasing height within the canopy (Figs. 4c and 5b).

Fig. 11 shows the effects of source locations on the maximum escape fraction ($\mathrm{EF}_{\max}$). Simulations in which particles are released in R1 and R2 yield much higher $\mathrm{EF}_{\max}$ than particles released in an infinite canopy (Fig. 11a). This suggests that particles from sources at the canopy leading edge are more likely to spread beyond the source canopy than sources in the fully developed region. In particular, most particles released in R1 escape the canopy region, giving

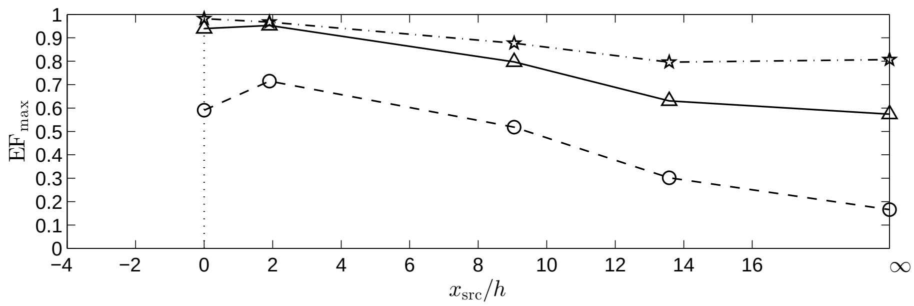

Figure 11: The maximum escape fraction ($\mathrm{EF}_{\max}$) against normalized streamwise source location (x_{src}/h). Results for particles released in the case of an infinite canopy ($x_{\mathrm{src}}/h \to \infty$) are from Pan et al. (2014a). *Dash lines with pentagrams, solid lines with triangles, and dash-dot lines with circles* indicate results for particles released at $z_{\mathrm{src}}/h = 1$, $2/3$, and $1/3$, respectively.

$\mathrm{EF}_{\max} \approx 1$. This is because most escape occurs at $x/h \leq 7$, the region where deposition on the canopy and ground is negligible (*red and green dash and solid lines* in Fig. 10*b*, *c*).

5. Discussion

The effects of mean vertical advection and canopy-shear-layer vortices (characterized by $\overline{w}$ and $z(\mathrm{Sk}_{u,\max})$, respectively) on vertical transport of particles are revealed through the growth rate of the mean plume height and the rate of deposition of particles on the ground. The mean plume height near the source ($\overline{z}$ at $(x - x_{\mathrm{src}})/h < 4$; Fig. 9*a*) grows faster for particles released at the canopy top as the source is moved towards the leading edge (*dash lines*), but grows faster for particles released in the lower canopy as the source is moved towards the fully developed region (*dash-dot lines*). The rapid growth of $\overline{z}$ with downwind distance for particles released at the top of R1 reveals the effect of strong positive mean vertical advection (*red* and *cyan dash lines* in Fig. 9*a*). In the fully developed region (R5 and R6), mean vertical advection becomes minor, while fully-developed canopy-shear-layer vortices dominate the vertical transport of particles. Specifically, the vertical transport processes in upper and lower canopies are dominated by sweeps and ejections, respectively (Finnigan et al., 2009). Note that sweeps ($u' > 0$, $w' < 0$) and ejections ($u' < 0$, $w' > 0$) are defined by turbulent velocity fluctuations ($u' = u - \overline{u}$, $w' = w - \overline{w}$). For particles released at the top of R5 (*blue dash line*), $\overline{z}$ is pushed down near the source, but rises again further downwind, which is similar to the behaviour of $\overline{z}$ for particles released at the top of an infinite canopy (*black dash line*). For particles released in the lower canopy, the increase of $\overline{z}$ with downwind distance is promoted by ejections associated with the canopy-shear-layer vortices, as well as the removal of particles by deposition on canopy elements and on the ground. Both mechanisms become stronger as the source is moved downwind from the leading edge, enhancing the growth of $\overline{z}$ (*dash-dot lines*). For particles released at the intermediate level (*solid lines*), the growth of $\overline{z}$ is enhanced by positive mean vertical advection that increases as the source is moved towards the leading edge as well as the deposition of particles that increases as the source is moved towards the fully-developed region. Therefore the growth of $\overline{z}$ does not show a monotonic dependence on the streamwise location of the source.

For a fixed streamwise release location, lowering the release height increases the fraction of particles removed by deposition on the ground (F_{Φ_G}; Fig. 10*c*). For a fixed release height, the rate of ground deposition is affected by mean vertical advection. Given a small settling velocity ($w_s/u_\star = 0.04 \ll 1$), particles released in R1 and R3 do not deposit on the ground until the plume enters the region where the flow within the canopy has been fully adjusted ($F_{\Phi_G} \approx 0$ at $x/L_c < 7$; *red*, *green* and *cyan dash and solid lines* in Fig. 10*c*). In the fully developed region, the positive mean vertical velocity becomes negligible, allowing downward transport of particles from upper to lower canopies. Ground deposition rates for particles released in R1 and R3 are similar to one another and are all lower than that for particles released in R5 (*blue dash and solid lines* in Fig. 10*c*). For particles released in the lower canopy, more particles released at $x_{\text{src}}/h = 0$ were removed by ground deposition than those released at $x_{\text{src}}/h = 2$ (*red and green dash lines* in Fig. 10*c*), showing the effect of negative mean vertical velocity at $-0.2 < x/h < 1.2$, $z/h < 1/2$. For release in R4 and R6, fewer particles were removed by ground deposition as the source is moved towards the leading edge, showing the effect of positive mean vertical velocity within these regions. Note that the patterns of ground deposition may change as the settling velocity increases. For example, particles released in R1 and R3 with a greater settling velocity may deposit on the ground before the plume enters the fully developed region.

6. Conclusions

The canopy leading edge affects the dispersion of particles through the development of the IBL and the adjustment of flow field within the canopy. The geometry of the mean plume away from the source becomes similar for particles released from different regions, as the mean plume height ($\overline{z}$) and depth (σ_z) become independent from the source location at ($(x - x_{\mathrm{src}})/h > 16$). The development of the IBL influences the growth rates of $\overline{z}$ and σ_z. Specifically, because mean shear within the IBL near the leading edge is greater than that above an infinite canopy, the growth rates of $\overline{z}$ and σ_z are lower than those for the case of an infinite canopy.

The escape fraction is an appropriate factor to rescale the source strength for long distance dispersal. In particular, the escape of fungal spores from plant canopies is an important controlling factor on the development of plant disease epidemics that involve aerial dispersal of inoculum (Aylor and Ferrandino, 1985; Madden et al., 2007). Simulation results show that most particle escape from the canopy region occurs close to the source ($(x - x_{\mathrm{src}})/h < 10$). The adjustment of flow field within the canopy impacts the escape of particles released inside the canopy. For a typical wind condition corresponding to $u_\star \approx 0.5$ m s^{-1}, the main flow characteristics as well as deposition and escape of particles close to the source are summarized in Tabel 1 for release from the different regions shown in Fig. 7. The adjustment length for deposition of particle on canopy elements is comparable with that for the flow, whereas the adjustment lengths for particle escape and deposition on the ground are greater than that for the flow. Determination of the adjustment length for particle escape requires further studies with sources at downwind distances greater than $x/L_c = 7$ from the leading edge.

Acknowledgements

This research is supported by the National Science Foundation (NSF) grant AGS1005363.

References

Alben, S., Shelley, M., Zhang, J., 2002. Drag reduction through self-similar bending of a flexible body. Nature 420, 479–481.

Aylor, D.E., Ferrandino, F.J., 1985. Escape of urediniospores of *Uromyces phaseoli* from a bean field canopy. Phytopathology 75, 1232–1235.

Aylor, D.E., Flesch, T.K., 2001. Estimating spore release rates using a Lagrangian Stochastic simulation model. J. Appl. Meteorol. 40, 1196–1208.

Bailey, B.N., Stoll, R., 2013. Turbulence in sparse, organized vegetative canopies: A large-eddy simulation study. Boundary-Layer Meteorol. doi:10.1007/s10546-012-9796-4.

Belcher, S.E., Finnigan, J.J., Harman, I.N., 2008. Flows through forest canopies in complex terrain. Ecol. Appl. 18, 1436–1453.

Belcher, S.E., Jerram, N., Hunt, J.C.R., 2003. Adjustment of a turbulent boundary layer to a canopy of roughness elements. J. Fluid Mech. 488, 369–398.

Bou-Zeid, E., Meneveau, C., Parlange, M.B., 2005. A scale-dependent Lagrangian dynamic model for large eddy simulation of complex turbulent flows. Phys. Fluids 17, 025105. Doi:10.1063/1.1839152.

Bouvet, T., Loubet, B., Wilson, J.D., Tuzet, A., 2007. Filtering of windborne particles by a natural windbreak. Boundary-Layer Meteorol. 123, 481–509.

Table 1: The main flow characteristics as well as deposition and escape of particles close to the source for release from different regions shown in Fig. 7 for a typical wind condition corresponding to $u_\star \approx 0.5$ m s^{-1}. Here F_{S_p} and F_{Φ_G} are fractions of particles removed by deposition on canopy elements and the ground, evaluated away from the source (i.e., at $(x - x_{src})/h > 10$). The *subscript* "∞" indicates results for particles released inside an infinite canopy.

Region	Flow Characteristics	Deposition	Escape
1	Strong mean wind Strong positive mean vertical velocity	$F_{S_p} \approx 0$ $F_{\Phi_G} \approx 0$	$\mathrm{EF}_{\max} \approx 1$
2	Strong mean wind Weak mean vertical velocity (negative and positive)	$0 < F_{S_p} < F_{S_p,\infty}$ $0 < F_{\Phi_G} < F_{\Phi_G,\infty}$	$\mathrm{EF}_{\max} \gg \mathrm{EF}_{\max,\infty}$
3	Deceleration of mean wind Development of canopy-shear-layer vortices Positive mean vertical velocity	$0 < F_{S_p} < F_{S_p,\infty}$ $0 < F_{\Phi_G} < F_{\Phi_G,\infty}$	$\mathrm{EF}_{\max} > \mathrm{EF}_{\max,\infty}$
4	Deceleration of mean wind Development of small-scale turbulence Positive mean vertical advection	$0 < F_{S_p} < F_{S_p,\infty}$ $0 < F_{\Phi_G} < F_{\Phi_G,\infty}$	$\mathrm{EF}_{\max} \gg \mathrm{EF}_{\max,\infty}$
5	Fully adjusted mean wind Strong sweeps associated with fully developed canopy-shear-layer vortices Negligible mean vertical velocity	$F_{S_p} \approx F_{S_p,\infty}$ $F_{\Phi_G} \approx F_{\Phi_G,\infty}$	$\mathrm{EF}_{\max} \approx \mathrm{EF}_{\max,\infty}$
6	Fully adjusted mean wind Fully developed small-scale turbulence Ejections associated with fully developed canopy-shear-layer vortices Negligible mean vertical velocity	$F_{S_p} \approx F_{S_p,\infty}$ $0 < F_{\Phi_G} < F_{\Phi_G,\infty}$	$\mathrm{EF}_{\max} > \mathrm{EF}_{\max,\infty}$

Chamecki, M., 2013. Persistence of velocity fluctuations in non-Gaussian turbulence within and above plant canopies. Phys. Fluids 25, 1–14.

Chamecki, M., Meneveau, C., Parlange, M.B., 2008. A hybrid spectral/finite-volume algorithm for large-eddy simulation of scalars in the atmospheric boundary layer. Boundary-Layer Meteorol. 128, 473–484.

Chamecki, M., Meneveau, C., Parlange, M.B., 2009. Large eddy simulation of pollen transport in the atmospheric boundary layer. J. Aerosol Sci. 40, 241–255.

Chen, Z., Jiang, C., Nepf, H., 2013. Flow adjustment at the leading edge of a submerged aquatic canopy. Water Resour. Res. 49, 5537–5551.

Chester, S., Meneveau, C., Parlange, M.B., 2007. Modeling turbulent flow over fractal trees with renormalized numerical simulation. J. Computational Phys. 225, 427–448.

Di-Giovanni, F., Kevan, P.G., 1991. Factors affecting pollen dynamics and its importance to pollen contamination: a review. Can. J. For. Res. 21, 1155–1170.

Dupont, S., Brunet, Y., 2008a. Edge flow and canopy structure: a large-eddy simulation study. Boundary-Layer Meteorol. 126, 51–71.

Dupont, S., Brunet, Y., 2008b. Influence of foliar density profile on canopy flow: a large-eddy simulation study. Agric. For. Meteorol. 148, 976–990.

Dupont, S., Brunet, Y., 2009. Coherent structures in canopy edge flow: a large-eddy simulation study. J. Fluid Mech. 630, 93–128.

Ferrandino, F.J., Aylor, D.E., 1984. Settling speed of clusters of spores. Phytopathology 74, 969–972.

Finnigan, J.J., 2000. Turbulence in plant canopies. Ann. Rev. Fluid Mech. 32, 519–571.

Finnigan, J.J., Shaw, R.H., Patton, E.G., 2009. Turbulence structure above a vegetation canopy. J. Fluid Mech. 637, 387–424.

Gleicher, S.C., Chamecki, M., Isard, S.A., Pan, Y., Katul, G.G., 2014. Interpreting three-dimensional spore concentration measurements and escape fraction in a crop canopy using a coupled Eulerian-Lagrangian Stochastic model. Agric. For. Meteorol. 194, 118–131.

Irvine, M.R., Gardiner, B.A., Hill, M.K., 1997. The evolution of turbulence across a forest edge. Boundary-Layer Meteorol. 84, 467–496.

Judd, M.J., Raupach, M.R., Finnigan, J.J., 1996. A wind tunnel study of turbulent flow around single and multiple windbreaks, part i: velocity fields. Boundary-Layer Meteorol. 80, 127–165.

de Langre, E., Gutierrez, A., Cossé, J., 2012. On the scaling of drag reduction by reconfiguration in plants. C. R. Mecanique 340, 35–40.

Lee, X., 2000. Air motion within and above forest vegetation in non-ideal conditions. For. Ecol. Management 135, 3–18.

Madden, L.V., Hughes, G., van den Bosch, F., 2007. The study of plant disease epidemics. American Phytopathological Society (APS Press), St Paul, MN. 421 pp.

McCartney, H.A., 1994. Dispersal of spores and pollen from crops. Grana 33, 76–80.

Morse, A.P., Gardiner, B.A., Marshall, B.J., 2002. Mechanisms controlling turbulence development across a forest edge. Boundary-Layer Meteorol. 103, 227–251.

Nieveen, J.P., El-Kilani, R.M.M., Jacobs, A.F.G., 2001. Behaviour of the static pressure around a tussock grassland–forest interface. Agric. For. Meteorol. 106, 253–259.

Pan, Y., Chamecki, M., Isard, S.A., 2013. Dispersion of heavy particles emitted from area sources in the unstable atmospheric boundary layer. Boundary-Layer Meteorol. 146, 235–256.

Pan, Y., Chamecki, M., Isard, S.A., 2014a. Large-eddy simulation of turbulence and paticle dispersion inside the canopy roughness sublayer. J. Fluid Mech. 753, 499–534.

Pan, Y., Follett, E., Chamecki, M., Nepf, H., 2014b. Strong and weak, unsteady reconfiguration and its impact on turbulence structure within plant canopies. *Phys. Fluids*, (in press).

Poggi, D., Porporato, A., Ridolfi, L., Albertson, J.D., Katul, G.G., 2004. The effect of vegetation density on canopy sub-layer turbulence. Boundary-Layer Meteorol. 111, 565–587.

Raupach, M.R., 1983. Near-field dispersion from instantaneous sources in the surface layer. Boundary-Layer Meteorol. 27, 105–113.

Raupach, M.R., 1989. Applying lagrangian fluid mechanics to infer scalar source distributions from concentration profiles in plant canopies. Agric. For. Meteorol. 47, 85–108.

Raupach, M.R., Finnigan, J.J., Brunet, Y., 1996. Coherent eddies and turbulence in vegetation canopies: the mixing-layer analogy. Boundary-Layer Meteorol. 78, 351–382.

Rominger, J., Nepf, H.M., 2011. Flow adjustment and interior flow associated with a rectangular porous obstruction. J. Fluid Mech. 680, 636–659.

Taylor, G.I., 1921. Diffusion by continuous movements. Proceedings of the London Mathematical Society 20, 196–211.

Van Breugel, P.B., Klaassen, W., Moors, E.J., 1999. Fetch requirements near a forest edge. Phys. Chem. Earth 24, 125–131.

Wilson, J.D., Ward, D.P., Thurtell, G.W., Kidd, G.E., 1982. Statistics of atmospheric turbulence within and above a corn canopy. Boundary-Layer Meteorol. 24, 495–519.

Yang, B., Morse, A.P., Shaw, R.H., Paw U, K.T., 2006a. Large-eddy simulation of turbulent flow across a forest edge. part ii: momentum and turbulent kinetic energy budgets. Boundary-Layer Meteorol. 121, 433–457.

Yang, B., Raupach, M.R., Shaw, R.H., Paw U, K.T., Morse, A.P., 2006b. Large-eddy simulation of turbulent flow across a forest edge. Part I: flow statistics. Boundary-Layer Meteorol. 120, 377–412.